Low-rank tensor completion with spatial-spectral consistency for hyperspectral image restoration

XIAO Zhiwen and ZHU Hu*

School of Communications and Information Engineering, Nanjing University of Posts and Telecommunications, Nanjing 210023, China

(Received 24 October 2022; Revised 4 February 2023)

Hyperspectral image (HSI) restoration has been widely used to improve the quality of HSI. HSIs are often impacted by various degradations, such as noise and deadlines, which have a bad visual effect and influence the subsequent applications. For HSIs with missing data, most tensor regularized methods cannot complete missing data and restore it. We propose a spatial-spectral consistency regularized low-rank tensor completion (SSC-LRTC) model for removing noise and recovering HSI data, in which an SSC regularization is proposed considering the images of different bands are different from each other. Then, the proposed method is solved by a convergent multi-block alternating direction method of multipliers (ADMM) algorithm, and convergence of the solution is proved. The superiority of the proposed model on HSI restoration is demonstrated by experiments on removing various noises and deadlines.

Document code: A **Article ID:** 1673-1905(2023)07-0432-5

DOI https://doi.org/10.1007/s11801-023-2182-2

Hyperspectral images (HSIs) can provide hundreds of contiguous spectral bands containing a wealth of spatial and spectral information[1]. As a result, HSI is used in many fields, including biomedicine, urban planning and many others. During acquisition, however, HSI is inevitably contaminated by mixing noise due to the unique physical design and limitations of the imaging mechanism[2,3]. This severely degrades image quality and limits the accuracy of subsequent processing tasks. Therefore, recovery as a pre-processing step for HSI applications is very important and challenging[4].

In the early years, many restoration methods are proposed by using the vectorization or matrixing of HSIs data, such as the K-singular value decomposition (K-SVD) method, nonlocal algorithm, and locally linear embedding (LLE) method. However, this kind of method does not consider the correlations between spatial regions or band and band, so the restoration performances are affected. HSI is imaged by a spectral sensor using different wavelengths of light on the same object, so the HSI data is highly correlated, i.e., the HSI data is of low rank. In order to be able to exploit the spectral features of HSI, a number of methods based on matrix low-rank (LR) priors have emerged[5-7]. Their main idea is to columnarize each band of the HSI into a vector, the HSI is then expanded into a low-rank matrix, and the low-rank prior of the HSI is then approximated by minimizing the rank of the matrix[3].

Inevitably, the matrixing operation described above destroys the intrinsic structure of the HSI. In most LR-based methods, the HSI data is always divided into patches and then rearranged into two-dimensional (2D) matrices resulting in the loss of inter-three-dimensional (3D) structural information. Tensor-based methods are proposed for restoring the HSI by modeling the HSI data as a 3D tensor. Tensor rank is most typically defined as completely positive (CP) rank[8] and Tucker rank, CP rank being defined as the minimum number of ranks required to represent a third-order tensor. However, calculating the CP for a given tensor is a difficult problem. The Tucker[9] rank is a vector in which the kth element is the rank of the mod k expansion matrix. However the unfolding operation in the Tucker decomposition also destroys the intrinsic structure of the tensor[10].

The spectral low-rank prior is the most widely used prior in hyperspectral recovery tasks. In contrast, there is still much room for improvement in the definition of tensor rank in existing studies. For example, the spectral and spatial dimensions have their own inherent low-rank structure, which may not be fully explored by existing models. On the other hand, there is some scope for optimisation of the form of the inscription of the tensor rank. Therefore, we propose a spatial-spectral consistency regularized low-rank tensor completion (SSC-LRTC) method, which not only can remove noise, but also can complete the HSI data. A convergent multi-block alternating direction method of multipliers (ADMM) algorithm is derived for the proposed SSC-LRTC model, and the existence of the solution and its convergence are demonstrated. In order to retain the advantages of the

*E-mail: zhuhu@njupt.edu.cn

direct generalization of the alternating direction multiplier method in numerical experiments, while ensuring the convergence of the iterative sequence generated by the algorithm, the ADMM is modified so that the iterative sequence generated by the algorithm converges. During each iteration, the variables are grouped so that the iterations are updated serially within the group and solved in parallel between the groups. This has the advantage of using the most recent iteration information possible, while minimising the time required for computation.

Given HSI data $\boldsymbol{H} \in \mathbb{R}^{M\times N\times B}$, we use $\boldsymbol{M}$ and $\boldsymbol{N}$ to denote the height and width of the image of each band, and use B to denote the number of spectral bands. Generally, the observed HSI data suffer from degradation, such as noise, or deadlines. Supposing the observed value of $\boldsymbol{H}$ is $\overline{\boldsymbol{H}} \in \mathbb{R}^{M\times N\times B}$ described as

$$\overline{\boldsymbol{H}} = \boldsymbol{H} + \boldsymbol{N}, \tag{1}$$

where $\boldsymbol{N} \in \mathbb{R}^{M\times N\times B}$ includes various degradations.

HSI restoration needs to obtain a clean HSI $\boldsymbol{H}$ from the observed HSI $\overline{\boldsymbol{H}}$. Generally, the HSI without noise $\boldsymbol{H}$ has the property of low rank, in order to get better HSI image restoration results, let $\boldsymbol{H} = \boldsymbol{M}_i, i = 1,2...N$ and $\boldsymbol{Z}$=$\boldsymbol{DH}$. We propose an SSC-LRTC model as follows

$$\min_{\boldsymbol{H}} \sum_{i=1}^{N} \left\|\boldsymbol{M}_{i(i)}\right\|_* + \frac{\varepsilon}{2}\left\|\boldsymbol{H} - \overline{\boldsymbol{H}}\right\|_F^2 + \frac{\beta}{2}\left\|\boldsymbol{Z}\right\|_F^2,$$

$$\text{s.t. } \boldsymbol{H} = \boldsymbol{M}_I, \boldsymbol{Z} = \boldsymbol{DH}, I = 1,2,...N. \tag{2}$$

The minimizer of Eq.(2) exists. In addition, it is global and unique. Let $\boldsymbol{Q} = (\boldsymbol{H},\boldsymbol{Z},\boldsymbol{M}_i, i = 1,2...N)$, and then Eq.(2) can be written as

$$\min L(\boldsymbol{H},\boldsymbol{Z},\boldsymbol{M}_1,...,\boldsymbol{M}_N) = \sum_{i=1}^{N}\left\|\boldsymbol{M}_{i(i)}\right\|_* + \frac{\varepsilon}{2}\left\|\boldsymbol{H} - \overline{\boldsymbol{H}}\right\|_F^2 + \frac{\beta}{2}\left\|\boldsymbol{Z}\right\|_F^2 + \delta_{\boldsymbol{Q}}(\boldsymbol{H},\boldsymbol{Z},\boldsymbol{M}_1,...,\boldsymbol{M}_N), \tag{3}$$

where $\delta_{\boldsymbol{Q}}(\boldsymbol{H},\boldsymbol{Z},\boldsymbol{M}_1,...,\boldsymbol{M}_N)$ is the indicator function of $\boldsymbol{Q}$, which can be defined as (for example)

$$\delta_{\boldsymbol{Q}}(\boldsymbol{H},\boldsymbol{Z},\boldsymbol{M}_1,...,\boldsymbol{M}_N) = \begin{cases} 0 & \text{if}(\boldsymbol{H},\boldsymbol{Z},\boldsymbol{M}_1,...,\boldsymbol{M}_N) \in \boldsymbol{Q} \\ +\infty & \text{otherwise} \end{cases}. \tag{4}$$

The minimizer of Eq.(3) exists and is global. Moreover, since $J(\boldsymbol{H},\boldsymbol{Z},\boldsymbol{M}_1,...,\boldsymbol{M}_N)$ is strongly convex, the minimizer of Eq.(3) is unique. In the following, we consider the concrete form of a dual problem.

$$\min_{\boldsymbol{H}} \frac{\varepsilon}{2}\left\|\boldsymbol{H} - \overline{\boldsymbol{H}}\right\|_F^2 - \left\langle \sum_{i=1}^{N}\boldsymbol{U}_i - \boldsymbol{D}^{\mathrm{T}}\boldsymbol{y}, \boldsymbol{H}\right\rangle. \tag{5}$$

Let $\sum_{I=1}^{N}\boldsymbol{U}_I - \boldsymbol{D}^{\mathrm{T}}\boldsymbol{y} = \boldsymbol{S}$ and $C_i := \{\boldsymbol{M}_{i|} \mid \left\|\boldsymbol{M}_{i(i)}\right\| \le 1\}$, and the dual problem of Eq.(3) is

$$\min_{\boldsymbol{y},\boldsymbol{S}} \frac{1}{2\varepsilon}\left\|\boldsymbol{S}\right\|_F^2 + \left\langle \boldsymbol{S}, \overline{\boldsymbol{H}}\right\rangle + \frac{1}{2\beta}\left\|\boldsymbol{y}\right\|_F^2 + \left(\sum_{i=1}^{V}\delta_{C_i}(\boldsymbol{M}_i)\right). \tag{6}$$

The augmented Lagrangian function of Eq.(6) is given by

$$L(\boldsymbol{M}_i,\boldsymbol{U}_i,\boldsymbol{y},\boldsymbol{S},\boldsymbol{T},\boldsymbol{Z}_i) = \frac{1}{2\varepsilon}\left\|\boldsymbol{S}\right\|_F^2 + \left\langle \boldsymbol{S},\overline{\boldsymbol{H}}\right\rangle + \frac{1}{2\beta}\left\|\boldsymbol{y}\right\|_F^2 + \left(\sum_{i=1}^{V}\delta_{C_i}(\boldsymbol{M}_i)\right) + \left\langle \boldsymbol{T}, \sum_{i=1}^{N}\boldsymbol{U}_i - \boldsymbol{D}^{\mathrm{T}}\boldsymbol{y} - \boldsymbol{S}\right\rangle + \sum_{i=1}^{N}\left\langle \boldsymbol{Z}_i, \boldsymbol{M}_i - \boldsymbol{U}_I\right\rangle + \frac{\rho}{2}\left\|\sum_{i=1}^{N}\boldsymbol{U}_i - \boldsymbol{D}^{\mathrm{T}}\boldsymbol{y} - \boldsymbol{S}\right\|_F^2 + \frac{\rho}{2}\sum_{i=1}^{N}\left\|\boldsymbol{M}_i - \boldsymbol{U}_i\right\|_F^2. \tag{7}$$

For $\boldsymbol{S}$, we have

$$\min_{\boldsymbol{S}} \frac{1}{2\varepsilon}\left\|\boldsymbol{S}\right\|_F^2 + \left\langle \boldsymbol{S},\overline{\boldsymbol{H}}\right\rangle - \left\langle \boldsymbol{T},\boldsymbol{S}\right\rangle + \frac{\rho}{2}\left\|\sum_{i=1}^{N}\boldsymbol{U}_i - \boldsymbol{D}^T\boldsymbol{y} - \boldsymbol{S}\right\|_F^2. \tag{8}$$

The minimizer of Eq.(8) is

$$\boldsymbol{S} = \frac{\varepsilon\rho}{\varepsilon\rho+1}\left(\sum_{i=1}^{N}\boldsymbol{U}_i - \boldsymbol{D}^{\mathrm{T}}\boldsymbol{y}\right) + \frac{\varepsilon\rho}{\varepsilon\rho+1}(\boldsymbol{T} - \overline{\boldsymbol{H}}). \tag{9}$$

For $\boldsymbol{M}_i$, we have

$$\min_{\boldsymbol{M}_i} \delta_{C_i}(\boldsymbol{M}_i) + \frac{\rho}{2}\left\|\boldsymbol{M}_i - \boldsymbol{U}_i + \frac{1}{\rho}\boldsymbol{Z}_i\right\|_F^2. \tag{10}$$

Let $\boldsymbol{\varepsilon}_i := \boldsymbol{U}_i - \boldsymbol{Z}_i / p$ and $\boldsymbol{\varepsilon}_{i(i)} = \boldsymbol{U}_i\boldsymbol{\Sigma}_i\boldsymbol{V}_i^{\mathrm{T}}$, where $\boldsymbol{\Sigma}_i$ is a diagonal matrix whose size is the same with $\boldsymbol{\varepsilon}_{i(i)}$, and its ith primary diagonal element of $\boldsymbol{\Sigma}_i$ denotes as σ_i. Thus

$$\boldsymbol{P}_i = \boldsymbol{U}_i \min\{\boldsymbol{\Sigma}_i, \boldsymbol{I}_i\}\boldsymbol{V}_i^{\mathrm{T}}, \tag{11}$$

where $\boldsymbol{I}_i$ is a diagonal matrix with the same size of $\boldsymbol{\Sigma}_i$, and the primary diagonal elements are 1. The result of $\min\{\boldsymbol{\Sigma}_i, \boldsymbol{I}_i\}$ is a matrix whose ith primary diagonal entry is $\min\{\sigma_i, 1\}$ with other entries equaling 0. The minimizer of Eq.(10) is given by

$$\boldsymbol{M}_i = \mathrm{Fold}_i(\boldsymbol{P}_i), \tag{12}$$

where is the mode-i fold operator. Then, we discuss the computation about $\boldsymbol{U}_i$.

For $\boldsymbol{U}_i$, we have

$$\min_{\boldsymbol{U}_i}\left\langle \boldsymbol{T} - \boldsymbol{Z}, \boldsymbol{U}_i\right\rangle + \frac{\rho}{2}\left\|\sum_{i=1}^{N}\boldsymbol{U}_i - \boldsymbol{D}^{\mathrm{T}}\boldsymbol{y} - \boldsymbol{S}\right\|_F^2 + \frac{\rho}{2}\left\|\boldsymbol{M}_i - \boldsymbol{U}_i\right\|_F^2. \tag{13}$$

The minimizer of Eq.(13) is

$$\boldsymbol{U}_i = \frac{1}{2}\left(\boldsymbol{M}_i + \frac{1}{P}(\boldsymbol{Z}_i - \boldsymbol{T})\right) - \frac{1}{2}\left(\sum_{j=1, j\ne i}^{N}\boldsymbol{U}_j - \boldsymbol{D}^{\mathrm{T}}\boldsymbol{y} - \boldsymbol{S}\right). \tag{14}$$

For $\boldsymbol{y}$, we obtain

$$\min_{\boldsymbol{y}} \frac{1}{2\beta}\left\|\boldsymbol{y}\right\|_F^2 - \left\langle \boldsymbol{T}, \boldsymbol{D}^{\mathrm{T}}\boldsymbol{y}\right\rangle + \frac{\rho}{2}\left\|\sum_{i=1}^{N}\boldsymbol{U}_i - \boldsymbol{D}^{\mathrm{T}}\boldsymbol{y} - \boldsymbol{S}\right\|. \tag{15}$$

The minimizer of Eq.(15) is given by

$$\left(\frac{1}{\beta}\boldsymbol{I}+\rho\boldsymbol{D}\boldsymbol{D}^{\mathrm{T}}\right)\boldsymbol{y}=\rho\boldsymbol{D}\left(\sum_{i=1}^{N}\boldsymbol{U}_i-\boldsymbol{S}+\frac{1}{\rho}\boldsymbol{T}\right). \tag{16}$$

We apply the multi-block ADMM to solve Eq.(6). We can observe that one block ($M_1,\ldots,M_N$) is nonsmooth and the other blocks are the convex quadratic functions in Eq.(6).

Thus, we can obtain a convergent optimal $\{\boldsymbol{M}_1^k,\ldots,\boldsymbol{M}_N^k, \boldsymbol{U}_1^k,\ldots,\boldsymbol{U}_N^k,\boldsymbol{y}^k,\boldsymbol{S}^k\}$ solution to Eq.(6), and $\{\boldsymbol{T}^k,\boldsymbol{Z}_1^k,\ldots,\boldsymbol{Z}_N^k\}$ is an convergent optimal solution of the dual problem of Eq.(6), i.e., an optimal solution of Eq.(3).

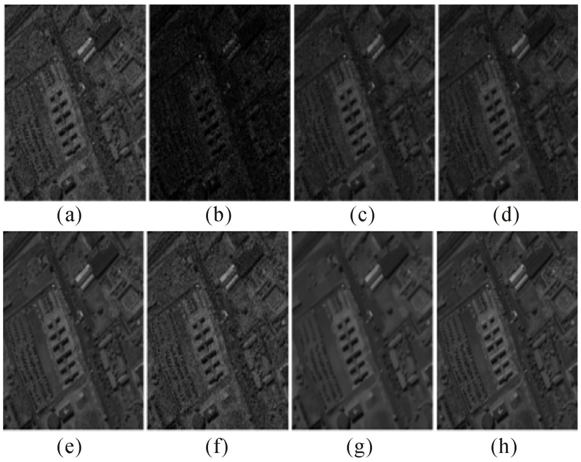

Fig.1 Restoration results of Pavia University with Gaussian noise: (a) Noisy image; (b) HaLRTC; (c) FaLRTC; (d) SiLRTC; (e) LRMR; (f) RLRTR; (g) LRTV; (h) SSC-LRTC

To show the performance of our method on HSI restoration, we perform several experiments on degraded HSI data and assess results quantitatively. We compare the results of our method with 5 state-of-the-art restorations methods, such as fast low-rank tensor completion (FaLRTC)[11], high accuracy low-rank tensor completion (HaLRTC)[11], and simple low-rank tensor completion (SiLRTC)[11], LRMR[12], RLRTR[13] and LRTV[14].

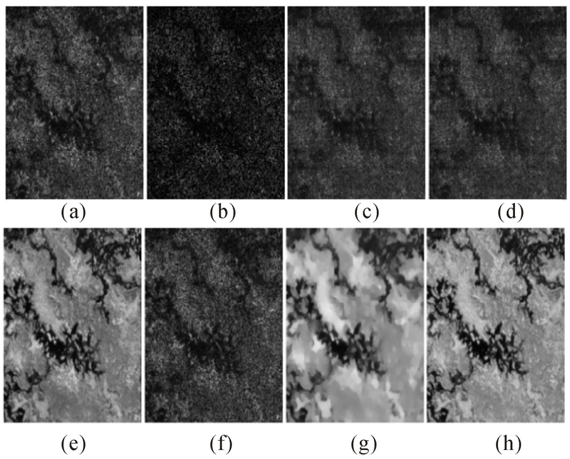

Fig.2 Restoration results of Botswana with speckle noise: (a) Noisy image; (b) HaLRTC; (c) FaLRTC; (d) SiLRTC; (e) LRMR; (f) RLRTR; (g) LRTV; (h) SSC-LRTC

Peak signal-to-noise ratio (*PSNR*), structural similarity index measurement (*SSIM*), and feature similarity index measurement (*FSIM*) are utilized to assess the performance of methods on each band. We give the mean value of the three kinds of evaluation indexes, *MPSNR*, *MSSIM*, and *MFSIM*.

Two HSI data, Pavia University and Botswana are used for simulation. The original image of the Pavia University Scene has 103 spectral bands and the size of the image of each band is 610×340 pixels. Botswana data has 145 spectral bands and images of each band have the size of 1 476×256. In our experiments, the sub-image of Pavia University Scene with the size of 340×340×103 and that of Botswana with the size of 256×256×115 are used. Then, we add Gaussian noise, speckle noise and deadlines to the two HSI data respectively for testing.

We set ε=0.1, β=0.15, τ=1.2, ρ=12 in the proposed method and they are updated with iteration. Firstly, Gaussian noise whose mean equals 0 and variance equals 0.01 is added to Pavia University and Botswana HSI, and restore them using HaLRTC, FaLRTC, SiLRTC, RLRTR, LRMR, LRTV methods, and the proposed SSC-LRTC method.

As shown, the original HSI was heavily contaminated in terms of image recognition and overall quality. After restoration, most of the noise was removed. However, HaLRTC, FaLRTC and SiLRTC are more suitable for low-intensity Gaussian noise removal. LRMR and RLRTR are better at suppressing Gaussian noise, but cannot remove strong impulse noise. In some denoising bands, there is still over-smoothing of the image and loss of texture information. LRTV also achieves good denoising results, but the denoising results in regions with rich texture information are not good enough compared to SSC-LRTC. The method in this paper smooths out more local detail with clearer local contours. The visual effects and metrics analysis show a significant improvement in the effectiveness of our proposed method over other methods, further demonstrating the effectiveness and rationality of our improved method.

In this paper, a spatially and spectrally consistent regularized low-rank tensor complementation model is proposed for noise removal and complementation of HSI data. Firstly, an SSC regularisation method is proposed

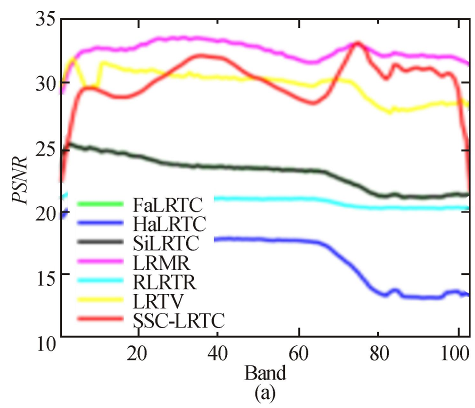

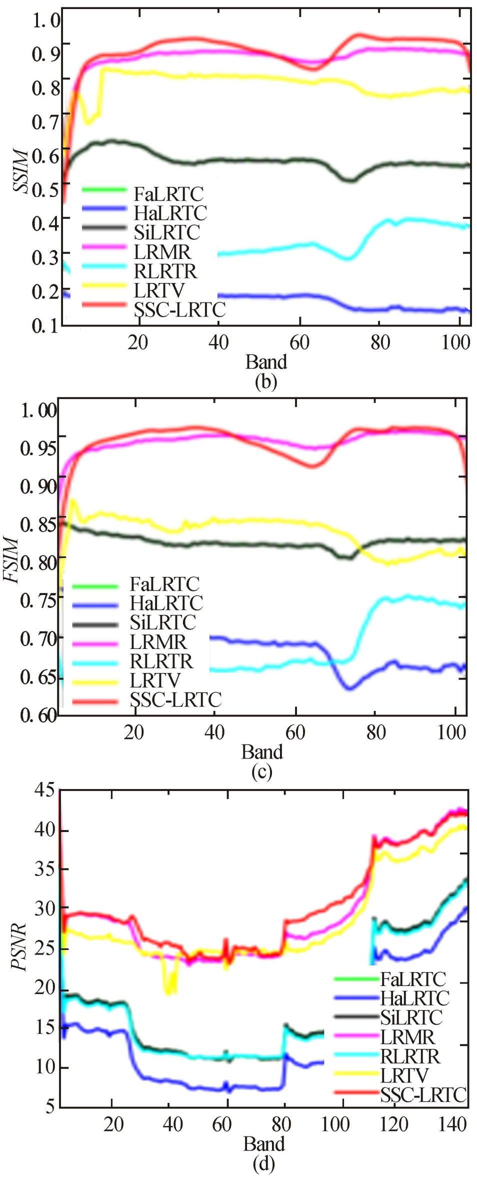

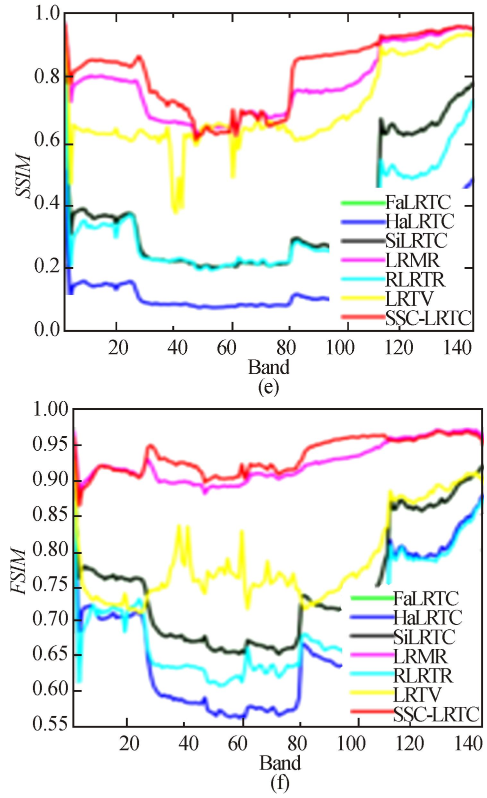

Fig.3 Evaluation values of indexes for noise removal: Results of (a) *PSNR*, (b) *SSIM* and (c) *FSIM* of Pavia University HSI data (Gaussian); Results of (d) *PSNR*, (e) *SSIM* and (f) *FSIM* of Botswana HSI data (speckle)

to help recover missing data from HSIs by considering the differences between images of different bands. Then, a convergent multi-block ADMM algorithm is derived to solve the model and prove the existence and convergence of the solution. Finally, various denoising experiments are conducted to verify the superiority of the method.

Tab.1 Mean values of quantitative indexes for dead line removal

Image	Index	FaLRTC	HaLRTC	SiLRTC	LRMR	RLRTR	LRTV	SSC-LRTC
Pavia University (*X*-direction)	*MPSNR*	25.030 6	22.272 5	24.943 3	17.369 2	17.341 6	17.444 4	**27.206 4**
	MSSIM	0.634 7	0.502 2	0.624 6	0.013 6	0.010 6	0.030 0	**0.869 6**
	MFSIM	0.755 1	0.595 7	0.748 2	0.554 5	0.473 4	0.573 8	**0.927 0**
Pavia University (*Y*-direction)	*MPSNR*	21.083 9	21.110 5	21.069 7	15.746 8	15.724 6	15.805 3	**26.792 5**
	MSSIM	0.591 3	0.595 4	0.595 4	0.012 4	0.009 7	0.034 3	**0.895 7**
	MFSIM	0.718 4	0.720 9	0.714 7	0.544 7	0.455 2	0.560 9	**0.936 6**
Botswana (*X*-direction)	*MPSNR*	29.129 7	18.325 2	29.337 5	18.321 7	18.315 9	18.391 1	**34.199 6**
	MSSIM	0.726 0	0.034 7	0.733 1	0.034 5	0.033 9	0.043 1	**0.931 8**
	MFSIM	0.828 8	0.587 2	0.834 1	0.587 2	0.585 9	0.589 7	**0.958 4**
Botswana (*Y*-direction)	*MPSNR*	28.336 1	17.902 4	28.514 8	17.885 8	17.873 6	17.963 5	**33.702 7**
	MSSIM	0.705 5	0.034 3	0.712 2	0.032 6	0.031 6	0.041 7	**0.935 2**
	MFSIM	0.823 3	0.588 2	0.827 6	0.596 4	0.535 1	0.588 5	**0.962 3**

The method in this paper has some advantages and achieves some results in the application of HSI recovery, but is of course subject to certain limitations. The higher computational complexity with long processing time can lead to poor applicability in applications, and forms such as parallel computing should be considered in subsequent research to improve the generalisability of model applications.

Ethics declarations

Conflicts of interest

The authors declare no conflict of interest.

References

[1] ZENG H, XIE X, NING J. Hyperspectral image denoising via global spatial-spectral total variation regularized nonconvex local low-rank tensor approximation[J]. Signal processing, 2021, 178：107805.

[2] ZENG H, XIE X, CUI H, et al. Hyperspectral image restoration via global L 1-2 spatial-spectral total variation regularized local low-rank tensor recovery[J]. IEEE transactions on geoscience and remote sensing, 2020, 59(4)：3309-3325.

[3] ZHENG Y B, HUANG T Z, ZHAO X L, et al. Mixed noise removal in hyperspectral image via low-fibered-rank regularization[J]. IEEE transactions on geoscience and remote sensing, 2019, 58(1)：734-749.

[4] MA A, ZHONG Y, ZHAO B, et al. Semisupervised subspace-based DNA encoding and matching classifier for hyperspectral remote sensing imagery[J]. IEEE transactions on geoscience and remote sensing, 2016, 54(8)：4402-4418.

[5] CAO X, ZHAO Q, MENG D, et al. Robust low-rank matrix factorization under general mixture noise distributions[J]. IEEE transactions on image processing, 2016, 25(10)：4677-4690.

[6] WANG J L, HUANG T Z, MA T H, et al. A sheared low-rank model for oblique stripe removal[J]. Applied mathematics and computation, 2019, 360：167-180.

[7] ZHENG Y B, HUANG T Z, JI T Y, et al. Low-rank tensor completion via smooth matrix factorization[J]. Applied mathematical modelling, 2019, 70：677-695.

[8] TICHAVSKÝ P, PHAN A H, CICHOCKI A. Numerical CP decomposition of some difficult tensors[J]. Journal of computational and applied mathematics, 2017, 317：362-370.

[9] LI Y F, SHANG K, HUANG Z H. Low Tucker rank tensor recovery via ADMM based on exact and inexact iteratively reweighted algorithms[J]. Journal of computational and applied mathematics, 2018, 331：64-81.

[10] JIANG T X, NG M K, ZHAO X L, et al. Framelet representation of tensor nuclear norm for third-order tensor completion[J]. IEEE transactions on image processing, 2020, 29：7233-7244.

[11] LIU J, MUSIALSKI P, WONKA P, et al. Tensor completion for estimating missing values in visual data[J]. IEEE transactions on pattern analysis and machine intelligence, 2013, 35(1)：208-220.

[12] ZHANG H, HE W, ZHANG L, et al. Hyperspectral image restoration using low-rank matrix recovery[J]. IEEE transactions on geoscience and remote sensing, 2013, 52(8)：4729-4743.

[13] WANG Y, PENG J, ZHAO Q, et al. Hyperspectral image restoration via total variation regularized low-rank tensor decomposition[J]. IEEE journal of selected topics in applied earth observations and remote sensing, 2017, 11(4)：1227-1243.

[14] SHI F, CHENG J, WANG L, et al. LRTV：MR image super-resolution with low-rank and total variation regularizations[J]. IEEE transactions on medical imaging, 2015, 34(12)：2459-2466.